Correspondence to:
S. Vanden Broucke,
sam.vandenbroucke@ees.kuleuven.be

New insights in the capability of climate models to simulate the impact of LUC based on temperature decomposition of paired site observations

Sam Vanden Broucke[1], Sebastiaan Luyssaert[2], Edouard L. Davin[3], Ivan Janssens[4], and Nicole van Lipzig[1]

[1]Department of Earth and Environmental Sciences, KU Leuven, Leuven, Belgium, [2]Le Laboratoire des Sciences du Climat et de l'Environnement (LSCE), Gif-sur-Yvette, France, [3]Institute for Atmospheric and Climate Science, ETH Zürich, Zürich, Switzerland, [4]Research group of Plant and Vegetation Ecology (PLECO), Department of Biology, University of Antwerp, Antwerp, Belgium

Abstract In this study, we present a new methodology for evaluating the biogeophysical impact of land use change (LUC) in regional climate models. For this, we use observational data from paired eddy covariance flux towers in Europe, representing a LUC from forest to open land (deforestation). Two model simulations with the regional climate model COSMO-CLM[2] (The Consortium for Small-Scale Modelling model in climate mode COSMO-CLM coupled to the Community Land Model CLM) are performed which differ only in prescribed land use for site pair locations. The model is evaluated by comparing the observed and simulated difference in surface temperature (T_s) between open land and forests. Next, we identify the biogeophysical mechanisms responsible for T_s differences by applying a decomposition method to both observations and model simulations. This allows us to determine which LUC-related mechanisms were well represented in COSMO-CLM[2], and which were not. Results from observations show that deforestation leads to a significant cooling at night, which is severely underestimated by COSMO-CLM[2]. It appears that the model is missing one crucial impact of deforestation on the nighttime surface energy budget: a reduction in downwelling longwave radiation. Results are better for daytime, as the model is able to simulate the increase in albedo and associated surface cooling following deforestation reasonably well. Also well simulated, albeit underestimated slightly, is the decrease in sensible heat flux caused by reduced surface roughness. Overall, these results stress the importance of differentiating between daytime and nighttime climate when discussing the effect of LUC on climate. Finally, we believe that they provide new insights supporting a wider application of the methodology (to other regional climate models).

1. Introduction

Research has shown that land use change (LUC) can have a significant biogeophysical impact on climate in the regions in which it occurs [*Bonan*, 2008; *Bala et al.*, 2007; *Davin and de Noblet-Ducoudré*, 2010; *Mahmood et al.*, 2014], and if large enough, may cause global effects [*Werth and Avissar*, 2002, 2005; *Hasler et al.*, 2009; *Medvigy et al.*, 2013]. It is therefore essential that the biogeophysical impact of LUC is modeled correctly in climate models. Currently, modelers rely mostly on standalone usage of land surface models (LSMs) to evaluate performance over different land use types [e.g., *Viterbo and Beljaars*, 1995; *van den Hurk et al.*, 2000; *Krinner et al.*, 2005; *Abramowitz et al.*, 2008; *Lauwaet et al.*, 2008; *Stöckli et al.*, 2008; *Akkermans et al.*, 2012; *Demuzere et al.*, 2013]. In standalone or so-called offline runs, the LSM is uncoupled from the climate model's atmospheric component and is instead driven by local measured atmospheric conditions (e.g., incoming shortwave and longwave radiation, atmospheric temperature, and humidity) in single grid cell mode. Model performance is then evaluated by comparing the LSM's response to this prescribed atmosphere (in terms of surface energy fluxes) to the measured response. This exercise is usually repeated for a series of different land use types.

Although this method of evaluating is useful and necessary, it does not, by itself, represent a complete evaluation of LUC effects in climate models. First, the model's ability to simulate the impact of a transition in land use is not evaluated directly. Rather, it is implicitly assumed that if the LSM simulates the surface climatology of two distinct land use types adequately, it is able to simulate the impact of a transition in land use between these two types as well. However, acceptable model biases in the surface climatology for two land use types could still result in an unacceptably large bias in the modeled difference. Secondly, offline runs do not account for surface-atmosphere feedbacks, while model intercomparison studies have shown that these indirect LUC effects are important drivers in various current generation climate models [*Boisier et al.*, 2012, 2013].

It is therefore important to evaluate the impact of LUC in coupled land-atmosphere climate models as well. The need for such evaluation is further underscored by a recent model intercomparison project called LUCID (Project Land-Use and Climate, Identification of Robust Impacts) [*Pitman et al.*, 2009]. In this project, seven climate models are used to simulate the biogeophysical impact of historic forest clearing (from preindustrial to present-day times), using global simulations. Results for temperature are relatively consistent, with all but one out of seven models simulating a cooling in the Northern Hemisphere. Furthermore, all seven models simulate a decrease in available energy due to increased albedo [*Boisier et al.*, 2012]. However, the climate models disagree substantially on how the surface responds to this energy deficit. Although all models simulate a decrease in the sum of turbulent fluxes, the amount varies. The decrease in turbulent fluxes is higher in magnitude than the increase in albedo for some models and lower for others [*de Noblet-Ducoudré et al.*, 2012]. Also, models disagree substantially on the partitioning of the decrease in turbulent fluxes over latent and sensible heat. For example, despite the decrease in available energy, three models simulate an increase in summer latent heat flux for the Northern Hemisphere, while the others simulate the opposite response [*Pitman et al.*, 2009].

Several aspects of the impact of LUC in coupled land-atmosphere climate models have recently been evaluated. For example, the changes in albedo [*Boisier et al.*, 2013] and evapotranspiration (ET) [*Boisier et al.*, 2014] modeled in the LUCID simulations were compared to reconstructed change maps by Boisier et al. For albedo, *Boisier et al.* [2013] were able to determine if the bias of individual ensemble members was due to a bias in the extent of simulated snow cover or due to a bias in how both snow surface albedo and vegetated surface albedo was parameterized. The parameterization was shown to be more important than the snow cover extent. For ET, the model ensemble was shown to underestimate the decrease since preindustrial times [*Boisier et al.*, 2014]. However, uncertainty on the reconstructed ET decrease was reported to be high, not only due in part to the uncertainty in the observational ET data sets but also due to a large dependency on the adopted land use map. Moreover, preindustrial ET values were derived using present-day data for the environmental drivers (precipitation, radiation, etc.), so potential atmospheric feedbacks were not accounted for [*Boisier et al.*, 2014]. Also, it is worth noting that both of these evaluation studies focus on evaluating climate models using observational data for only one surface energy budget component at a time.

In addition, existing studies that evaluate the impact of LUC in coupled land-atmosphere climate models rarely distinguish between daytime and nighttime climate, instead limiting the analysis to daily means. However, large differences in physical properties exist between the convective and nocturnal planetary boundary layer. Therefore, it is likely that the response to LUC differs significantly between day and night. Furthermore, studies have detected a disproportionate nocturnal contribution to near surface warming in historic surface temperature records [*Karl et al.*, 1993; *Vose et al.*, 2005; *Nair et al.*, 2011]. Possible responsible factors include tropospheric aerosols, greenhouse gases, and clouds. LUC has been proposed as a possible factor as well [*Zhou et al.*, 2007]. It is therefore worthwhile to investigate if LUC has an impact on nighttime climate, and whether that impact is to dampen or enhance recent warming. If done using modeling studies, this means that climate models should be evaluated specifically for their ability to model the nighttime impact of LUC.

In this study, we present a new method for evaluating a climate model's ability to simulate the impact of LUC which extends above mentioned studies to a simultaneous evaluation of the impact of LUC on all surface energy budget components in a coupled land-atmosphere climate model. Our methodology consists of (1) a direct evaluation of the differences in surface climate instead of evaluating land use types separately, (2) online model simulations which account for atmospheric feedbacks, (3) a separate analysis of daytime and nighttime climate, (4) a simultaneous evaluation of all surface energy budget components, and (5) an evaluation of the models' capacity to reproduce the underlying processes following a LUC. Next, we apply this new methodology to a state of the art regional climate model.

2. Methods and Materials

2.1. Observational Data

The term land use change incorporates many possible transitions. Examples are forest clearing for wood production and/or agricultural use, reforestation of former agricultural areas, the conversion of natural

Table 1. Characteristics of Site Pairs Used in This Study[a]

Cluster Name	Latitude	Longitude	Site Name	Elevation (m)	Distance (km)	Data Availability	Land Use	IGBP Class	Climate Group
DK1	55.49	11.65	Soroe-LilleBogeskov	40	28.8	2004:2008	Mixed forest	DBF	Temperate
DK1	55.53	12.10	Risbyholm	10	28.8	2004:2008	Cropland	CRO	Temperate
DE1	50.96	13.57	Tharandt	380	8.5	2004:2008	Mixed forest (87% evergreen)	ENF	Temperate
DE1	50.89	13.52	Klingenberg	480	8.5	2004:2008	Cropland	CRO	Temperate
CZ1	49.50	18.54	Bily Kriz Beskidy	908	0.9	2004:2006	Young Norway spruce plantation	ENF	Temperate-continental
CZ1	49.50	18.54	Bily Kriz Grassland	855	0.9	2004:2006	Grassland (managed as meadow)	GRA	Temperate-continental
IT2	45.96	11.28	Lavarone	1343	19.3	2003:2008	Mixed coniferous forest	ENF	Temperate
IT2	46.02	11.05	Monte Bondone	1550	19.3	2003:2008	Grassland (managed as meadow)	GRA	Temperate
IT1	41.85	13.59	Collelongo	1550	6.2	2002:2008	Irregularly structured beech forest	DBF	Subtropical Mediterranean
IT1	41.90	13.61	Amplero	884	6.2	2002:2008	Pasture	GRA	Subtropical Mediterranean
ES1	39.35	−0.32	El Saler	10	7.8	2004:2006	Pine forest	ENF	Subtropical Mediterranean
ES1	39.28	−0.32	El Saler-Sueca	41	7.8	2004:2006	Cropland	CRO	Subtropical Mediterranean
PT1	38.54	−8.00	Mitra Tojal	250	7.4	2004:2005	Cork and holm oak	EBF	Subtropical Mediterranean
PT1	38.48	−8.02	Mitra Evora	190	7.4	2004:2005	Grassland	GRA	Subtropical Mediterranean

[a]List of site pairs used in this study, the distance between sites within a pair, and the years for which common measurements are available. Each site pair is assigned an acronym based on its location (e.g., DE1 is located in Germany) and consists of a forest and an open land site. In total, 14 sites were used to create 7 site pairs. International Geosphere-Biosphere Programme (IGBP) classes represented in this data set include deciduous broadleaf forests (DBF), evergreen needleleaf forests (ENF), evergreen broadleaf forests (EBF), grasslands (GRA), and croplands (CRO).

grasslands to irrigated agriculture, and (sub) urbanization. To demonstrate the methods, we focus on the climate impact of deforestation over Europe and deforestation as the transition from forest to open land.

Instead of selecting individual sites representing a variety of land use types, which would be the starting point of a more typical evaluation, we selected sites where an open land flux tower and a forest tower are located in close proximity. When located sufficiently close to each other, one can assume these site pairs share the same background climate conditions and ideally even the same weather, for example, timing of particular events, occurrence of heat waves, and extreme precipitation. Therefore, any differences in surface climate conditions between the two sites constituting a site pair (e.g., 2 m air temperature, evapotranspiration, and sensible heat flux) can be attributed to the difference in land use.

In order for observational sites to be selected, they have to (1) be located in the study domain, i.e., Europe, (2) consist of a forested site and an open land site which could be either a cropland or a grassland, (3) be located less than 35 km apart from each other. The 35 km was chosen in accordance with the spatial resolution of the model (see section 2.2), (4) have a common measurement period of at least 1 year, and finally, (5) have at least measurements of 2 m air temperature, net radiation, latent heat, and sensible heat fluxes.

In total, 14 sites in the FLUXNET database match these criteria and were subsequently combined in seven site pairs (Table 1 and Figure 1). The vegetation at the selected sites ranges from temperate, continental to subtropical Mediterranean, and contains diverse management regimes with the most common being yearly cutting for most of the meadows and occasional thinning at the forested sites. The forested sites include both deciduous and coniferous tree species.

The average linear distance between sites within a pair is 11.3 km; the average latitudinal distance between sites is 6.0 km. These values are in line with the average distances reported by other studies that use site pairs to study the impact of LUC [*Lee et al.*, 2011; *Baldocchi and Ma*, 2013; *Luyssaert et al.*, 2014; *Zhang et al.*, 2014]. Elevation differences within a pair range from
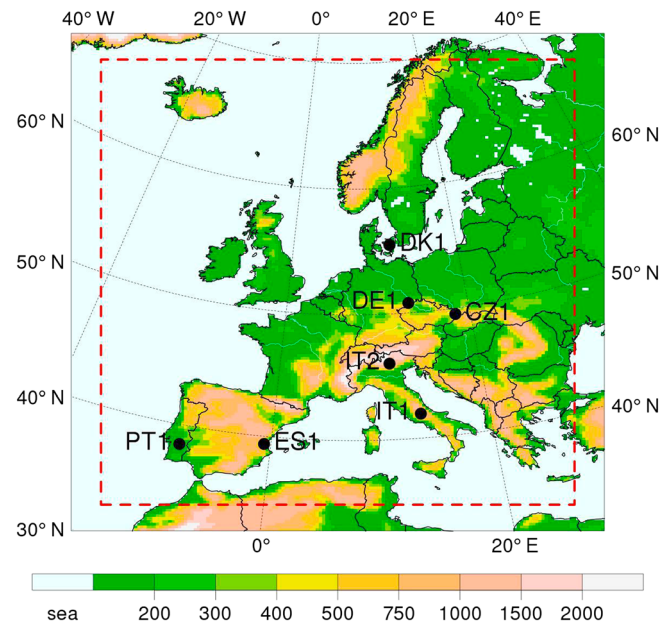
Figure 1. Topography of the model domain and location of the observational pairs. This map shows the model domain, including the relaxation zone, the area outside the red rectangle.

minor; i.e., the height difference between the site pairs in clusters DK1, DE1, CZ1, ES1, and PT1 is limited to 100 m or less to relatively large; i.e., Collelongo is located almost 700 m higher than Amplero, which are the two sites which form site pair IT1.

2.2. Models

The regional climate simulations analyzed in this study are performed with the COSMO-CLM[2] model [*Davin et al.*, 2011; *Davin and Seneviratne*, 2012]. COSMO-CLM[2] couples the atmospheric component of the regional climate model COSMO-CLM (version 4.8) to the Community Land Model version 3.5 (CLM3.5), the land surface component of the Community Earth System Model. COSMO-CLM 4.8 thus differs from the standard COSMO-CLM by replacing the relatively simple land surface component included in the model with the more comprehensive CLM 3.5.

Model evaluations show that the standard version of COSMO-CLM 4.8 meets all requirements to qualify as a state of the art regional climate model [*Keuler et al.*, 2012; *Kotlarski et al.*, 2014; *Vautard et al.*, 2013]. It has been used extensively over Europe for both regional climate modeling and numerical weather prediction [*Feldmann et al.*, 2013; *Lauwaet et al.*, 2013; *Baldauf et al.*, 2011] and has been applied to other major world regions as well [*Dosio et al.*, 2014; *Asharaf and Ahrens*, 2013; *Kothe et al.*, 2014; *Nikulin et al.*, 2012]. A recent model intercomparison study performed for a European model domain has shown that compared to standard COSMO-CLM, COSMO-CLM[2] improves performance for several climate variables, including cloud cover, surface temperature, and precipitation. The main factor explaining these performance improvements is a better partitioning of turbulent fluxes [*Davin et al.*, 2011; *Davin and Seneviratne*, 2012].

Both simulations were integrated using a horizontal resolution of 0.22° (~25 km), a vertical resolution of 32 pressure levels and a 120 s time step. The model grid covers all of western Europe (Figure 1) and consists of 170 × 180 pixels in, respectively, latitude and longitude. Both simulations were integrated from 1 July 2002 to 1 January 2009, a time period which covers the available observations and includes a 6 month spin-up period before the first available measurement year (2003). Initial and boundary conditions were derived from ERA-Interim Reanalysis data.

2.3. Model Experiment

In this study, the model experiment required two simulations. In the first simulation (the "forest" simulation), the seven pixels matching the seven locations of the observational pairs were prescribed as forest. In the second simulation (the "open land" simulation), the same seven pixels were set to grassland or crop depending on the surface above which the FLUXNET mast was installed.

When doing a standard simulation with CLM3.5, values that describe the land surface are derived from input data sets [*Lawrence and Chase*, 2007]. Surface input variables required for CLM3.5 include plant functional type (PFT), canopy top and bottom height, leaf area index (LAI), stem area index, soil color, and soil texture. For this study, three of these input variables were adapted to local measurement site conditions: PFT, canopy top height, and LAI. Values for these adaptations are summarized in Table 2. First, for PFT, one in four options was chosen depending on land use (forest or open land) and dominant tree species: needleleaf evergreen tree—temperate or broadleaf deciduous tree—temperate on the forest side, and C3 grass or crop on the open land side. Second, the input variable canopy top height was adapted to the

Table 2. List of Model Parameter Values for All FLUXNET Sites[a]

Cluster Name	Site Name	PFT	CTH	LAI$_{max}$
DK1	Soroe-LilleBogeskov	BDT-T	20	4.8
DK1	Risbyholm	Crop	0.5	1.4
DE1	Tharandt	NET-T	26.5	7
DE1	Klingenberg	Crop	0.5	2.4
CZ1	Bily Kriz Beskidy	NET-T	12.5	6.7
CZ1	Bily Kriz Grassland	C3 Grass	0.5	2.2
IT2	Lavarone	NET-T	30	8
IT2	Monte Bondone	C3 Grass	0.5	3.2
IT1	Collelongo	BDT-T	21.2	5
IT1	Amplero	C3 Grass	0.5	2.4
ES1	El Saler	NET-T	12	3.1
ES1	El Saler-Sueca	Crop	0.5	1.1
PT1	Mitra Evora	BDT-T	7	2.2
PT1	Mitra Tojal	C3 Grass	0.5	1.7

[a]Shows plant functional type (PFT), canopy top height (CTH), and summer maximum of leaf area index (LAI$_{max}$).

observational sites for the forest simulation only. For the open land simulation, the standard CLM3.5 value for grassland and cropland of 0.5 m was used. Finally, CLM3.5 uses a yearly cycle of LAI which is updated daily by interpolating between monthly values [*Oleson et al.*, 2004]. For the forest sites, these monthly LAI values were adjusted to match the local site conditions more closely.

2.4. Data Processing

The observational data sets were downloaded from the European Fluxes Database Cluster (http://www.europe-fluxdata.eu/). For this study, level 2 data products were used throughout. These data products provide values on a half-hourly timescale and are quality checked by the site PI but have not been through any gap filling. Further data processing was required for the aims of this study. For all variables three subsets were created: one subset containing daily mean values, another containing the daytime mean, and the last subset containing nighttime mean values. This approach enabled separately studying nighttime and daytime climate as well as evaluating the effect when this distinction is not made and daily means are used instead.

For the daily mean subset, a mean daily value was calculated for every variable from the half-hourly level 2 product. Days with measurement gaps longer than 3 h were removed from the data set. For the daytime mean subset, a mean daily value was calculated for all observation from 12:00 to 15:00 UTC. If one of the six half-hourly measurements within this window was missing, the whole day was omitted from the daytime mean subset. A similar procedure was used to calculate the nighttime subset, except here, the 00:00 to 03:00 UTC time window was used. All of the following data processing steps were performed on these three subsets:

1. Albedo and surface emissivity were calculated for sites with separate measurements for incoming and outgoing shortwave and longwave radiation. Surface albedo (α_s) was determined by computing the ratio between outgoing and incoming shortwave radiation for the daytime mean subset (12:00–15:00 UTC). Next, surface emissivity ε_s was derived from surface albedo using a simple linear equation ($\varepsilon_s = 0.16\,\alpha_s + 0.99$). This empirical relationship was derived from literature reported values of albedo and emissivity [*Juang et al.*, 2007].

2. For sites with separate measurements for incoming and outgoing longwave radiation, radiative surface temperature (T_s) was derived from outgoing longwave (LW$_{out}$) using Stefan Boltzman's equation (LW$_{out} = \varepsilon_s \sigma T_s^4$).

3. Observed energy budgets are rarely closed, and imbalances of up to 20% of available energy are common [*Wilson et al.*, 2002]. It has been suggested that one of the most prominent sources for this imbalance is an underestimation of the turbulent fluxes, caused by the fact that the eddy covariance method tends to miss or underestimate large-scale eddies [*Foken*, 2008]. Therefore, the surface energy budget (SEB) was closed by redistributing the imbalance term (incoming terms minus outgoing terms) to sensible and latent heat, with the fraction of the imbalance allocated to each term determined by the measured Bowen ratio (relative proportion of sensible to latent heat). Note that this means we assume the Bowen ratios for small- and large-scale eddies are similar. Although this might not hold in all cases [*Ruppert et al.*, 2006], the redistribution of the imbalance based on Bowen ratio is the only method easily applicable to our observational data set.

4. As we aim to compare the climatology of nearby sites, the difference between the values observed at the forest site and the nearby open land site were calculated. We chose to subtract the forest site value from the open land value, so the calculated difference value therefore reflects the change associated with deforestation. The output data from our model simulations was processed in a similar fashion with the

sole exception that by conception the energy budget of COSMO-CLM^2 is closed and no imbalance correction (see step (3)) was required.

2.5. Decomposition of Surface Temperature Change

To decompose the observed change in radiative surface temperature (T_s) between forested and open land sites, the method originally developed by *Juang et al.* [2007] was used. This method has been refined [*Luyssaert et al.*, 2014] and subsequently been applied by others [*Luyssaert et al.*, 2014; *Akkermans et al.*, 2014; *Thiery et al.*, 2015]. The decomposition uses the basic surface energy budget equation as its starting point:

$$\epsilon_s \sigma T_s^4 = [1 - \alpha_s]\mathrm{SW_{in}} + \mathrm{LW_{in}} - \mathrm{LE} - H - G - I \tag{1}$$

By reordering the equation and performing a first-order derivative, the decomposition equation for δT_s or the difference in surface temperature between two sites is obtained:

$$\delta T_s = \frac{1}{4\varepsilon\sigma T_s^3}\left[-\mathrm{SW_{in}}\delta\alpha_s + (1-\alpha_s)\delta\mathrm{SW_{in}} + \delta\mathrm{LW_{in}} - \delta\mathrm{LE} - \delta H - \delta G - \delta I - \sigma T_s^4\delta\varepsilon_s\right] \tag{2}$$

This equation is then applied to our site pairs, which reflect a local land use transition from forest to open land. Using the equation, we can attribute the change in surface temperature to eight factors:

1. *Albedo* (α_s). A positive value implies that the open land site is darker than the forest and therefore absorbs a larger fraction of the incident solar radiation.
2. *Incoming shortwave radiation* (SW_{in}). A positive value implies that the incoming shortwave radiation is higher over the open land site. Possible mechanisms could be feedbacks including changes in atmospheric moisture, atmospheric aerosol loading, cloud cover, etc.
3. *Incoming longwave radiation* (LW_{in}). A positive value implies that the incoming longwave radiation is higher over the open land site. Possible mechanisms could be changes in cloud cover, atmospheric aerosol loading, water vapor loading in the lower boundary layer, etc.
4. *Latent heat flux* (LE). A positive value implies that the latent heat flux, and therefore, the evaporative cooling of the surface, is lower for the open land site.
5. *Sensible heat flux* (H). A positive value implies a reduction in convective surface cooling.
6. *Ground flux* (G). A positive value implies reduced soil heat storage.
7. *The imbalance term* (I). The imbalance term accounts for the imbalance as discussed above as well for the omission of minor components of the energy budget such as heat storage in biomass, heat storage in subcanopy air mass, and energy used in photosynthesis. Ideally, this component should approach zero, but for observational data, this is almost never the case.
8. *The thermal emissivity of the surface* (ε_s). A positive value implies an increase in the surface emission of longwave radiation due to an increase in emissivity, with the surface more closely resembling a black-body radiation.

For the observational data subsets, the surface temperature decomposition equation was applied twice: once using the original uncorrected values for sensible and latent heat and then again using the values corrected for imbalance. The differences between these values can be interpreted as a measure of the uncertainty related to measuring turbulent fluxes.

Applying the equation to both observations and modeled site pairs results in a daily value for δT_s, calculated from the observed and modeled differences in all surface energy budget components. For COSMO-CLM^2, this calculated value matches the actual daily mean δT_s value closely across the board. However, this is not the case when the surface temperature decomposition equation is applied to our observational site pairs. Here large discrepancies exist between calculated and observed δT_s reflecting uncertainties in the measurements. Consequently, we can use the difference between the calculated and the observed value of δT_s as an estimate for data reliability.

As mentioned earlier, a surface energy budget closure imbalance of about 20% of available energy is common in measurements [*Wilson et al.*, 2002]. For our site pairs, this corresponds to an imbalance of about 11 W m^{-2}, or 2 K when translated to temperature using equation (2). Therefore, 2 K was chosen as a cutoff value for calculated minus observed δT_s ($\delta T_{scalc} - \delta T_{sobs}$). Days where ($\delta T_{scalc} - \delta T_{sobs}$) is lower than this cutoff value are deemed reliable; days that do not meet this criterion are not. This data reliability

Table 3. Data Availability[a]

			IT2	DE1	DK1	IT1	CZ1	PT1	ES1
Number of Years			6	5	5	5	3	2	3
T_a measurements	Entire year	0–24	97	93	96	67	38	70	88
		12–15	97	92	96	67	36	70	88
		0–3	97	92	96	66	35	69	87
	JJA	0–24	93	98	93	83	83	67	100
		12–15	92	97	92	81	78	67	100
		0–3	92	96	91	81	78	67	99
	DJF	0–24	97	85	98	43	0	67	74
		12–15	97	84	98	43	0	67	74
		0–3	96	84	98	42	0	67	74
LW_{out} measurements	Entire year	0–24	96	78	41	17	28	0	0
		12–15	96	77	41	16	27	0	0
		0–3	96	76	40	16	26	0	0
	JJA	0–24	91	75	39	27	55	0	0
		12–15	91	73	38	25	52	0	0
		0–3	91	73	38	26	51	0	0
	DJF	0–24	96	84	42	5	0	0	0
		12–15	95	83	42	5	0	0	0
		0–3	95	81	42	5	0	0	0
Reliable	Entire year	0–24	25	35	21	0	0	0	0
		12–15	6	29	19	0	0	0	0
		0–3	22	41	21	0	0	0	0
	JJA	0–24	24	44	14	0	0	0	0
		12–15	4	36	12	0	0	0	0
		0–3	0	52	15	0	0	0	0
	DJF	0–24	29	34	18	0	0	0	0
		12–15	10	30	17	0	0	0	0
		0–3	49	38	18	0	0	0	0

[a]Data availability for T_a, LW_{out}, and reliable decomposition results (see section 2.5) in percentage of days with observations. 0–24 denotes the entire day, 12–15 daytime, and 0–3 nighttime observations. JJA (June–August) and DJF (December–February) were used to distinguish between summer and winter months, respectively. Number of years denotes the number of years for which the sites within a pair have common measurements.

measure was applied separately to all three data subsets created for our observational site pairs. For a site pair, at least 25% of the days for which the decomposition method was applied had to pass the 2 K threshold to be included in the final data set.

2.6. Data Availability and Quality

Despite the length of the time series, our additional criteria to data quality and availability (see section 2.5) considerably reduced the size of the data (Table 3). For example, for the CZ1 site pair, 3 years of common measurements are available. However, only 38% of days within this common measurement period have T_a measurements for both sites within the site pair.

LW_{out} is an important variable because it is essential in calculating surface temperature (T_s). Since we use the difference between the calculated and the observed value of T_s as a measure for data reliability, this means that site pairs with no common measurements of LW_{out} cannot pass our reliability test. For most site pairs, however, LW_{out} is the variable with the least consistent coverage, and thus the most limiting. Two pairs (PT1 and ES1) out of seven have no common LW_{out} measurements at any time. For two other pairs (IT1 and CZ1) common measurements of LW_{out} are mostly restricted to summer. Coverages of ~40%, ~80%, and, ~95%, respectively, make DK1, DE1, and IT2 the only three pairs remaining for the core of the analysis. Site pairs DE1 and DK1 have the highest fraction, i.e., 55 to 75% of reliable measurements (Figure 2), where reliability is calculated as the number of days for which ($\delta T_{scalc} - \delta T_{sobs}$) is less than ±2 K. For the IT2 site pair, data reliability is lower overall, and less consistent across time of day.

A possible reason for the lower fraction of reliable site comparisons at site pairs IT2 is the substantial elevation difference of the sites within this pairs. For IT2, the open land site is located 210 m higher than the forest site. Whereas, height differences for DE1 and DK1 are only 100 and 30 m, respectively.
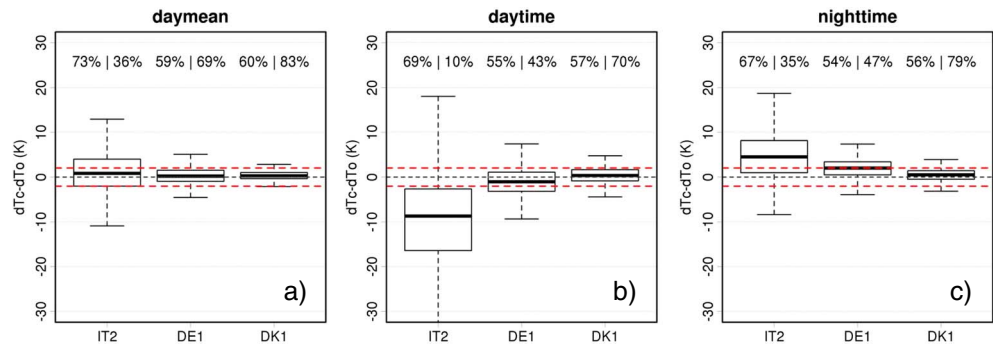
Figure 2. Box plots of calculated minus observed δT_s ($\delta T_{scalc} - \delta T_{sobs}$). The data reliability range (±2 K) is indicated in red. The percentage values printed over the box plots show two values: the percentage of days with LW_{out} measurements that have measurements for all surface energy budget terms (left-hand value) and the percentage of days with measurements of all surface energy budget terms that are deemed reliable (right-hand value).

It is, however, worth noting that despite the low percentages of high-quality data, sample size is adequate for our purpose thanks to the relatively high number of years with common measurements for these site pairs. The daily mean reliable year-round subset, for example, still contains 1570 days when summed across site pairs 1–3. The lowest absolute number of days can be found in the summer daytime mean subset, which still contains 243 entries (Table 3).

3. Results

3.1. Difference in Temperature

The yearly mean daytime difference in air temperature (δT_a, with T_a typically measured approximately 2 m above the vegetation canopy) does not differ significantly from zero ($p = 0.71$), being equal to about 0.02 K (Figure 3). Note that these values are uncorrected for the height difference between the sites within pairs. Based on a possible lapse rate range of 5.5–10 K/km, we calculated a weighted average δT due to height difference of -0.53 to -0.96 K. In the subsequent analysis, δT values in the 0 to -0.96 K range should therefore be considered to be insignificant from zero. The daytime δT_a due to deforestation is simulated reasonably well by COSMO-CLM[2]: agreement is strong, with the model replicating the observed seasonal cycle almost perfectly (Pearson correlation, 0.94). The difference in daytime T_s is characterized by a strong seasonal signal: in winter, δT_s for open land sites is cooler by about 1.5 K, while in spring and summer, open land sites are warmer by up to 3 K. Summer warming is stronger and longer in duration, dominating the yearly mean daytime δT_s signal. The model produces a seasonal pattern similar to observations: open land sites are cooler than forests in winter and warmer in summer. COSMO-CLM[2] does somewhat underestimate the magnitude of summer open land warming.

At nighttime, yearly mean nighttime δT_a equals about -1.3 K, suggesting that the atmosphere above open land is cooler than above forest with minimal seasonal variation. COSMO-CLM[2] does not succeed at simulating this observed nighttime δT_a, overestimating yearly mean nighttime δT_a by about 1.5 K. The difference in nighttime δT_s does show seasonal variation: in winter open land site T_s is lower by up to 5.5 K, while in late summer and fall, open land sites are still cooler but the difference is reduced to 2.5 K. It is worth noting, however, that the seasonal amplitude in nighttime δT_s is significantly smaller for the data set containing all data. Still, the fact that open land sites are cooler during nighttime than nearby forests is robust across pairs. Similar to nighttime δT_a, COSMO-CLM[2] does a poor job in simulating the observed nighttime δT_s with a bias of 4 K between the simulated and observed values. These nighttime biases are large enough to reverse the sign of nighttime δT_s compared to the observations: unlike in the observations, in our COSMO-CLM[2] simulations, open land sites are warmer than forests at night, especially in spring.

Finally, daily mean δT_a averages about -0.8 K, with little to no seasonal variation. It is driven primarily by the difference in nighttime temperature, which is considerably higher in magnitude than the observed daytime temperature difference. COSMO-CLM[2] overestimates daily mean δT_a by about 0.5 K due to the δT_a
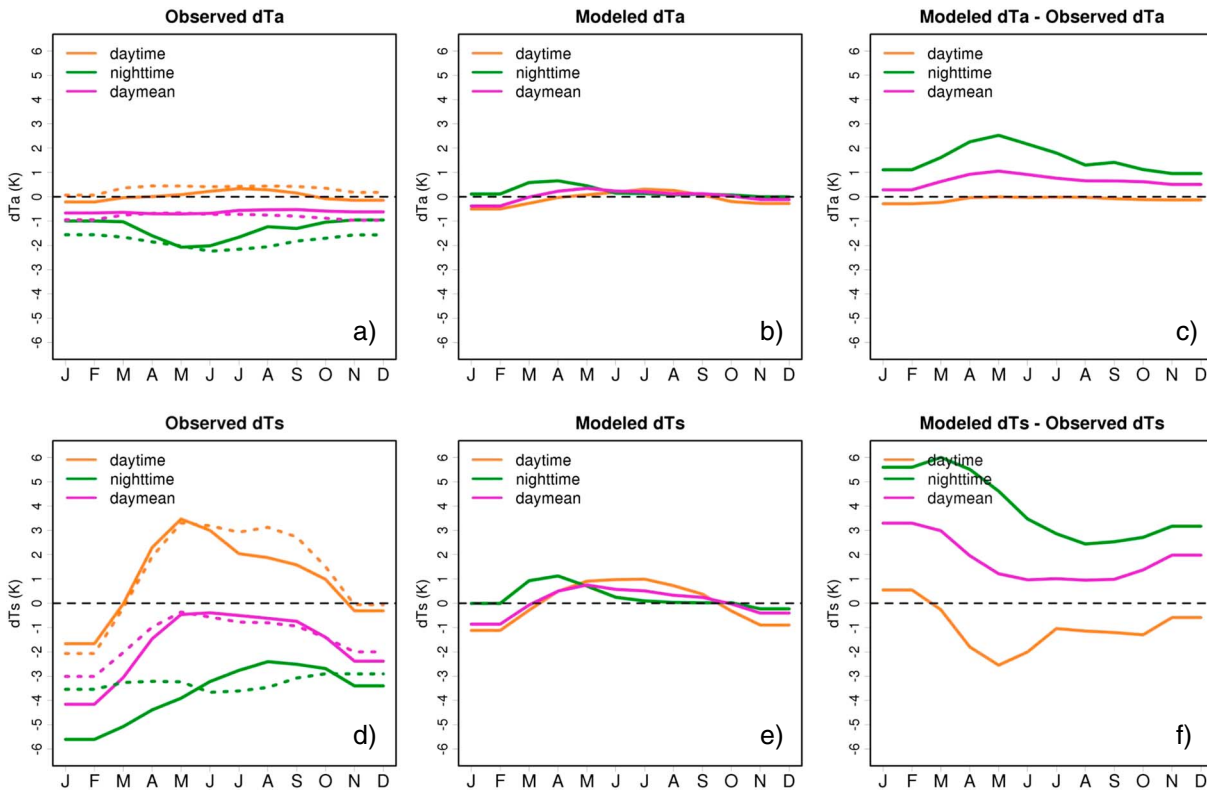
Figure 3. Mean seasonal cycle of (a) observed δT_a, (b) modeled δT_a, and (c) δT_a bias (modeled δT_a MINUS observed δTa). Mean seasonal cycle of (d) observed δT_s, (e) modeled δT_s, and (f) δT_s bias (modeled δT_s MINUS observed δT_s). For Figures 3a and 3d, the solid lines show the temperature difference for the data set containing only reliable measurements, while the dashed lines show the temperature difference when all available measurements are used. A 3 month running mean was applied to all time series.

overestimation at night. Daily mean δT_s is also negative year round. Its seasonal signal (about −3.5 K in winter, close to zero in summer) is determined mostly by daytime δT_s, while its sign (negative year round) is determined mostly by nighttime δT_s. In COSMO-CLM^2, daily mean δT_s is overestimated by about 2 K, again mainly because of the nighttime bias.

3.2. Surface Temperature Change Decomposition
3.2.1. Daytime/Summer

Using the δT_s decomposition equation, changes in T_s were attributed to changes in the components of the surface energy budget (Figure 4). For summer days, the difference in albedo between open land and forested sites appears to be a dominant factor in changes in surface temperature. Albedo is higher for open land sites, where the difference in albedo was estimated to be equivalent to a δT_s of −6 K. This difference is modeled accurately by COSMO-CLM^2 in both sign and magnitude (Figure 4a). For the observed pairs, summer days are thus characterized by a lower net radiation (R_{net}) at the open site compared to the forest. However, the surface responds to deforestation by simultaneously reducing the sensible heat flux (H), a reduction which, if isolated, would cause a surface heating of 6 to 8 K. This reduction in H is consistent with a decrease in surface aerodynamic roughness (R_s), common for deforestation. The reduction in H more than offsets the cooling through increased albedo, causing the observed surface warming of 2 K. Consistent with a decrease in surface aerodynamic roughness and possibly, due to a shallower rooting system, LE was also observed to decrease with an effect on T_s ranging between 0 and 5 K (corrected for lack of SEB closure and uncorrected, respectively).

The interplay between albedo-driven cooling and roughness-driven warming following deforestation is reasonably well represented in COSMO-CLM^2. Contrary to the observations, however, modeled warming due to a reduction in H does not exceed albedo cooling. In COSMO-CLM^2, both counteracting processes
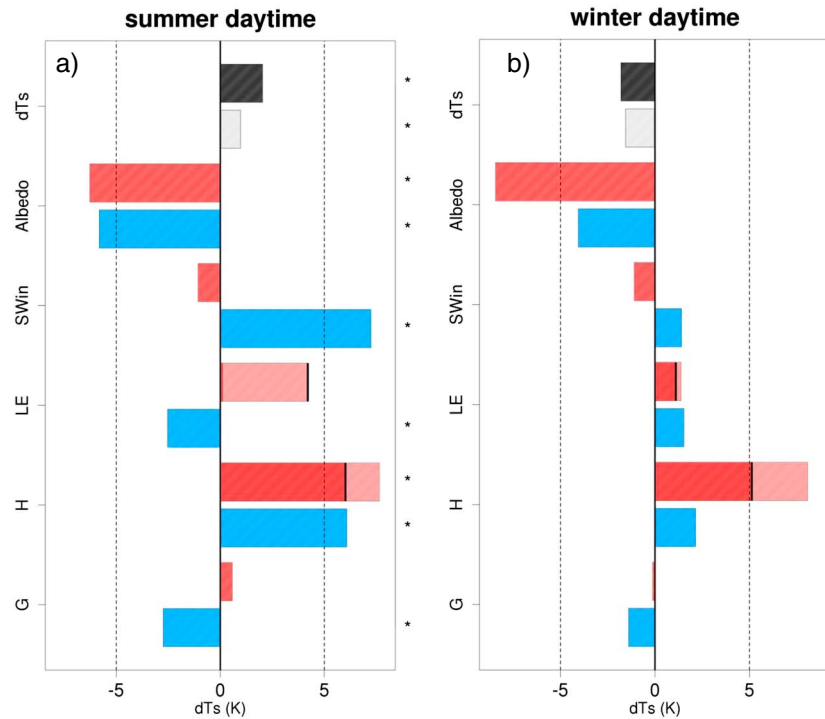
Figure 4. Surface temperature change decomposition for daytime (12–15 UTC), for (a) summer and (b) winter. All values represent the change associated with deforestation. The modeled and observed mean δT_s is shown on top where black is for the observed values and grey for modeled. The contributions to δT_s for the main components of the surface energy budget are shown in red for observed and blue for modeled values. For sensible and latent heat flux, δT_s was calculated using both the original values and the values corrected for surface energy imbalance. The resulting uncertainty is represented by the light colored portion of each bar. A black line indicates the δT_s value calculated with the uncorrected values for H and LE. δT_s terms which are significantly different from zero ($p = 0.05$) are marked by asterisks. For reasons of simplicity, components with an associated temperature change that have a yearly mean absolute δT_s value of less than 0.5 K across observations and model simulations were not shown. For daytime, this means surface emissivity and incoming longwave radiation.

are of equal magnitude (+6 K versus −6 K). The model and observations differ most in the difference in incoming shortwave radiation from the atmosphere (SW$_{in}$) to the vegetation. The difference due to SW$_{in}$ is small and statistically insignificant ($p = 0.50$) for the observational site pairs, but very important in our model simulations. In COSMO-CLM^2, increased SW$_{in}$ (+7 K) is offset only partially by increases in both LE and ground flux (G) (−2.5 K to −3 K each). The result is a surface warming of about 1 K. For summer days, COSMO-CLM^2 thus simulates a correct change in surface temperature due to deforestation, but the underlying processes are somewhat different.

As shown in Figure 5a, the increase in modeled incoming shortwave radiation present in our COSMO-CLM^2 simulations is a feature that is present in all seven site pairs, not just the three site pairs with reliable measurements included in the temperature change decomposition analysis. Figure 5a also shows that the increase is highest in summer and lowest in winter. The increase in SW$_{in}$ appears to be caused by a decrease in cloud cover (δ_{CLC}), and specifically, in medium-level (not shown) and low-level clouds (dCLC, Figure 5b). This is evidenced by the fact that the peak in δSW$_{in}$ seem to coincide well with the negative peak in δ_{CLC}.

3.2.2. Daytime/Winter

The effect of deforestation on winter surface temperature is simulated correctly in COSMO-CLM^2, with the model simulating a surface cooling of 2 K, consistent with observations (Figure 4b). Similar to summer daytime, the difference in albedo drives the observed and simulated changes. However, COSMO-CLM^2 underestimates the magnitude of the associated cooling of the open land compared to forest. The model simulates a δT_s due to albedo of about −4 K, as opposed to −8 K for the observations. This presents a departure from the model's behavior in summer, where the modeled effect of changes in albedo
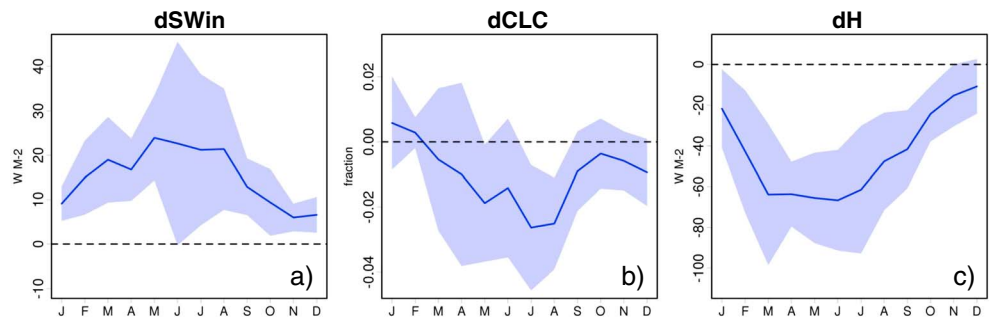
Figure 5. Seasonal cycle of modeled daytime difference for three variables: (a) incoming shortwave radiation (SW_{in}), (b) low-level cloud cover (CLC), and (c) sensible heat flux (H). The blue line shows the monthly mean over all seven site pairs. Also drawn is an area plot of ±1 standard deviation. All available data were used for these figures (not just days with reliable observations).

reasonably matched the observations. The difference in observed and modeled albedo is likely related to a mismatch between observed and simulated snow cover, rather than a deficiency in how plant canopy albedo is parameterized. This is supported by the fact that for the open land sites in our observational data set, 21% of winter days with reliable measurements have a surface albedo higher than 0.5, typical for a snow surface. In our model simulations, this is only the case for 5% of winter days.

The observational data show that deforestation is associated with a decrease in H, triggered by both the reduction in R_{net} and lower surface aerodynamic roughness and resulting in a surface warming of 5 to 8 K. COSMO-CLM^2 also simulates a decrease in H, albeit smaller in absolute value (2.5 K). However, relative to albedo cooling, the decrease in H is similar in both model and observations (66 to 100% of albedo cooling for the observations versus 60% of albedo cooling for COSMO-CLM^2). Finally, deforestation is characterized by a small decrease in LE in both observations and COSMO-CLM^2, triggered by a combination of lower R_{net}, lower surface aerodynamic roughness and a shallower rooting system. The model does not match the observed changes in SW_{in} and G though. Whereas observed SW_{in} shows a small decrease and no change in G, model simulations show a small increase in SW_{in} and a small increase in G.

Overall, we can conclude that COSMO-CLM^2 simulates the observed δT_s during winter days accurately and, moreover, is correct in its simulation of the underlying mechanisms: albedo-induced cooling partially offset by a decrease in sensible heat flux is the dominant mechanism during winter days for both model and observations. COSMO-CLM^2 does underestimate the magnitude of albedo-induced cooling due to an underestimation in the amount of snow events compared to observations.

3.2.3. Nighttime
During nighttime, open land sites are observed to be significantly cooler than nearby forested sites (Figure 6) during both summer (−2 K) and winter (−5 K). This LUC effect is completely missing from our COSMO-CLM^2 simulations. In COSMO-CLM^2, open land nighttime temperatures are statistically equal to nearby forest temperatures during summer ($p = 0.13$), and only slightly lower during winter. The biggest difference between model and observations is in the incoming longwave radiation component (LW_{in}). For our observational site pairs LW_{in} over the open land site is considerably lower than over the nearby forested site. The cooling associated with this reduction in LW_{in} ranges from 1.5 to 2.1 K, for summer and winter, respectively. In our model simulations, the cooling associated with this factor is smaller, ranging from 0.1 to 0.5 K.

Monthly box plots for the difference in nighttime incoming longwave radiation (δLW_{in}) are shown in Figure 7 for both model and observations. On the observational side, mean δLW_{in} across all reliable data equals $-7.8 \, W \, m^{-2}$ and is statistically different from zero ($p < 1E−15$). The 75th percentile of δLW_{in} is below zero for all but 3 months, pointing toward a broad yearlong trend of decreased LW_{in} following deforestation. On the other hand, COSMO-CLM^2 simulations are characterized by a mean δLW_{in} of only $-0.9 \, W \, m^{-2}$, a difference which is not statistically different from zero ($p = 0.10$). Therefore, we can conclude that in our simulations, no broad yearlong trend toward a decrease in LW_{in} exists.

Model and observations disagree over the change in G as well, and the disagreement observed in this component contributes to explaining why simulated and observed δT_s differ. In summer, both
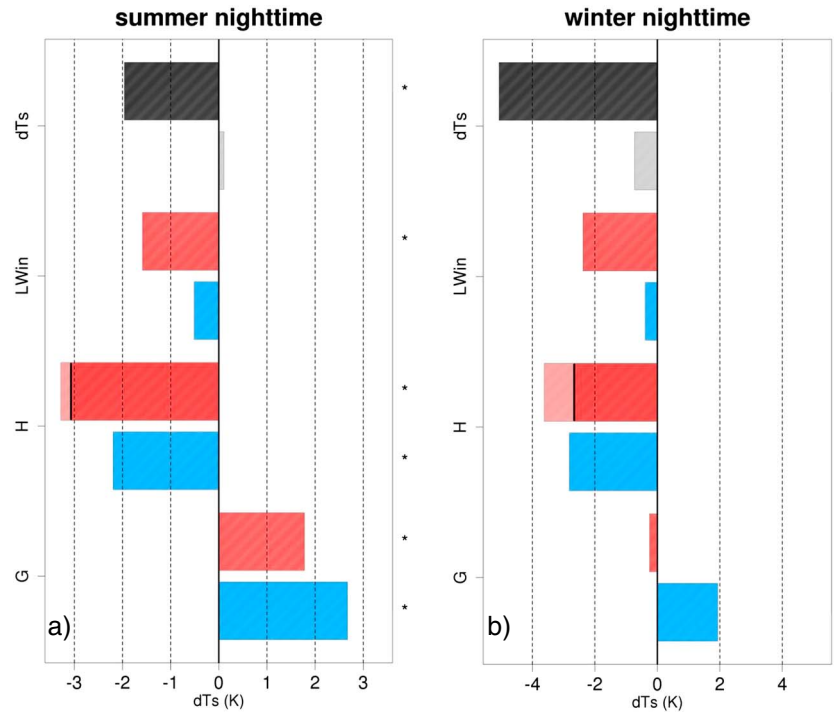
Figure 6. Surface temperature change decomposition for nighttime (00–03 UTC) for (a) summer and (b) winter. All values represent the change associated with deforestation. The modeled and observed mean δTs is shown on top where black is for the observed values and grey for modeled. The contributions to δT_s for the main components of the surface energy budget are shown in red for observed and blue for modeled values. For sensible and latent heat flux, δT_s was calculated using both the original values and the values corrected for surface energy imbalance. The resulting uncertainty is represented by the light colored portion of each bar. A black line indicates the δTs value calculated with the uncorrected values for H and LE. δT_s terms which are significantly different from zero ($p = 0.05$) are marked by asterisks. For reasons of simplicity, components with an associated temperature change that have a yearly mean absolute δT_s value of less than 0.5 K across observations and model simulations were not shown. For nighttime, this means surface emissivity, incoming shortwave radiation and latent heat flux.

observations and simulations have a lower (more negative) G for open land sites compared to forests. In other words, heat loss of soils to the surface is more important for open land than for forest. However, COSMO-CLM^2 overestimates this effect by almost 1 K. In winter, the observed difference in ground flux between open land and forested sites is significant on the 0.05 level but very small ($p = 0.01$), whereas in COSMO-CLM^2 open land sites still have more ground heat release, causing a surface warming of about 2 K.

The observed and modeled mean daily cycle of G during winter for forest and open land are shown in Figure 8. The observed G is characterized by minimal diurnal variation, remaining slightly negative throughout. This is true for both open land and forest sites, as both lines are virtually identical. Modeled G, however, is characterized by considerable diurnal variation, from highly positive during daytime to
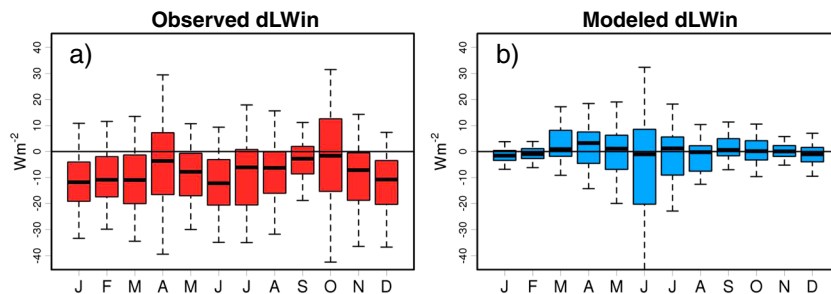
Figure 7. Box plots of difference in nighttime LW$_{in}$ (dLW$_{in}$) following deforestation for (a) observations and (b) COSMO-CLM^2 model simulations. Only reliable data were used.
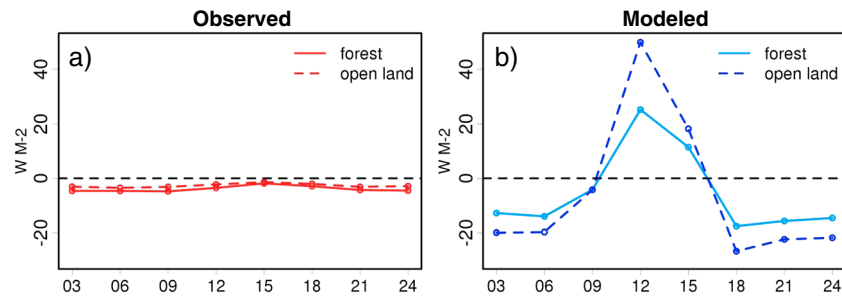
Figure 8. Mean daily cycle of ground flux during winter for (a) observations and (b) COSMO-CLM2 model simulations, for forest and open land sites. Mean over all site pairs. Only reliable data were used.

negative at night. Moreover, modeled G differs between forests and open land, resulting in a nighttime difference in surface warming not present in reality. It is worth noting that at least in part, this disagreement between model and observations could be related to the modeled underestimation in wintertime snow cover (as mentioned in section 3.2.2), since snow tends to insulate the soil column.

Observations and simulations do agree on the contribution caused by the sensible heat component (H). At night, as the surface cools, a stable reverse stratification usually forms in the nocturnal boundary layer. Turbulence can disrupt this stable stratification and bring heat from aloft to the surface. However, open land sites are characterized by a decreased surface roughness and thus, a decrease in turbulence. This is observed at our observational pairs: the open land sites are characterized by a higher H, which at night means less negative, leading to a mean cooling of 2.2 to 3 K compared to forests, depending on season. COSMO-CLM^2 is able to simulate this behavior with the associated cooling matching observations in winter and slightly underestimating this process by 0.8 K in summer.

4. Discussion

4.1. Daily Cycle of the Observed Temperature Difference Between Forest and Grassland

Owing to the strict requirements for data quality and availability, our study could only make use of three to seven observational pairs depending on the analysis. Representativeness of our analysis of few sites was tested against the body of literature on the topic. A strong latitudinal dependency of the drivers of δT is emerging from literature study. For the tropical zone, most studies agree that deforestation causes a warming of local climate because here, the warming effect of a decrease in evapotranspiration tends to outweigh the cooling effect of a higher albedo [e.g., *von Randow et al.*, 2004]. This first-order effect of deforestation has been successfully reproduced by several modeling studies [*Davin and de Noblet-Ducoudré*, 2010; *Nogherotto et al.*, 2013; *Akkermans et al.*, 2013, 2014; *Lejeune et al.*, 2014]. Conversely, in the boreal zone, most observational studies agree that deforestation leads to a cooling of local climate, because here, the increase in albedo due to the highly contrasting albedo during the snow season dominates the temperature response [e.g., *Randerson et al.*, 2006]. Temperate climate zones, such as in Europe where this study was located, are characterized by a δT response that is in between these two extremes. Just like in the tropical and boreal climate zones, open land surfaces tend to be brighter than forests, a cooling effect that increases with latitude due to the increasing presence of winter snow cover. Two other mechanisms have the potential to cause an opposing surface warming: a reduction in turbulent surface cooling due to reduced surface roughness and decreased evapotranspiration due to both reduced roughness and a shallower rooting system.

Despite observational evidence remaining limited, most studies using observational data for temperate regions (e.g., Europe, most of North America, and parts of Asia) agree on the aforementioned biogeophysical mechanisms (Table 4). Disagreement does exist over the sign of the yearly mean δT signal. Some observational studies conclude that winter cooling is strong enough to dominate the yearly mean δT signal, or in other words, that on a yearly mean-scale deforestation leads to surface cooling [*Lee et al.*, 2011; *Zhang et al.*, 2014]. *Baldocchi and Ma*, 2013 also report cooling, but the dominant mechanisms here are somewhat different. Other observational studies conclude that the summer decrease in LE and/or H

Table 4. Overview of Observational Studies Reporting the Effect of Deforestation on Both Surface Temperature and All Surface Energy Budget Terms

Study	Location	Temperature Variable	Time of Day	dT	Mechanism
Juang et al. [2007]	North Carolina	T_s	0–24	+1 K	Higher albedo more than offset by reduction in H/LE
			12–15	✗	✗
			0–3	✗	No separate explanation
Montes-Helu et al. [2009]	Northern Arizona	T_s	0–24	DJF −1 K, JJA +3 to +7 K	Higher albedo offset by reduction in H/LE, balance depending on season
			12–15	✗	✗
			0–3	✗	✗
Baldocchi and Ma [2013]	California	Potential T_a	0–24	−0.5 K	(DJF) reduction in H (JJA) higher-albedo offset by lower LE
			12–15	DJF −0.8 K, JJA +1.7 K	✗
			0–3	DJF −0.8 K, JJA −2.2 K	✗
Lee et al. [2011] and *Zhang et al.* [2014]	North America and East Asia, north of 45°N	T_a	0–24	−0.85 K, −0.95 K	Separate explanation for day/night
			12–15	0 K, 0 K	Higher albedo perfectly offset by reduction in H/LE
			0–3	−2 K, −2 K	Reduced turbulence
Lee et al. [2011] and *Zhang et al.* [2014]	North America and East Asia, south of 45°N	T_a	0–24	−0.21 K, −0.35 K	Separate explanation for day/night
			12–15	+1 K, +1.2 K	Higher albedo more than offset by reduction in H/LE
			0–3	−2 K, −1.9 K	Reduced turbulence

and associated summer warming following deforestation is strong enough to cause a positive yearly mean signal for δT [e.g., *Juang et al.*, 2007; *Montes-Helu et al.*, 2009].

The studies cited here are some of the only observational studies performed for temperate zones that simultaneously study the effect of deforestation on both surface temperature and the full surface energy budget. The fact that some studies associate deforestation with surface warming while others observe cooling supports the hypothesis that in temperate regions, the yearly mean δT signal is the results of opposing mechanisms and can go toward either warming or cooling depending on local conditions [*Pitman et al.*, 2011; *Luyssaert et al.*, 2014]. Interestingly, results from modeling studies using global climate model simulations tend be more one sided. These studies generally agree that deforestation in temperate regions leads to surface cooling [*Snyder et al.*, 2004; *Brovkin et al.*, 2006; *Bala et al.*, 2007; *Davin and de Noblet-Ducoudré*, 2010]. One possible reason could be the large scale of deforestation utilized in these simulations, when compared to the scale of deforestation typical for observational studies. These large-scale deforestations could trigger atmospheric and/or ocean feedbacks in global climate models that do not occur after deforestations smaller in scale (e.g., a sea ice feedback). Furthermore, we speculate that these model simulations do not fully capture the varied observed impact of deforestation because they lack the variety in land use subtypes present in reality.

The seven observational pairs used in this study are characterized by a yearly mean δT of about −2.5 K and are thus in line with the global climate modeling studies and other observational studies. However, it is worth noting that so far, we have only discussed the daily mean climate effect of deforestation. Few studies distinguish between daytime and nighttime climate when analyzing the effect of deforestation on temperature. Only two such studies could be found using observational data for climate zones similar to our European study area: a study for North America conducted by *Lee et al.* [2011] and a follow-up study performed by *Zhang et al.* [2014] for Eastern Asia. In concordance with our results, these studies confirm the importance of differentiating between daytime and nighttime climate when analyzing δT caused by deforestation.

Lee et al. [2011] compared 2 m air temperature for 37 open land/forest site pairs across North America. A surface energy budget analysis showed that daytime δT_a following deforestation is determined by the balance between two processes also described in this study: warming due to suppression of turbulent fluxes versus cooling due to increased albedo. For site pairs in the 28°–45°N latitudinal range the effect of these two processes on T_a offset

Table 5. Overview of the Biogeophysical Mechanisms Responsible for Observed and Modeled δT_s Values[a]

Reality	COSMO-CLM[2]
Effect of Deforestation on Daytime Climate	
Cooling due to lower surface albedo (α_s), which is offset by warming due to reduced surface roughness (R_s)	✓
?	Reduced $R_s \rightarrow$ reduced convective uplift $\rightarrow$ reduced CLC $\rightarrow$ increase in $SW_{in} \rightarrow$ surface warming (most prominent in JJA)
Effect of Deforestation on Nighttime Climate	
Reduced $R_s \rightarrow$ reduced turbulent mixing$\rightarrow$ surface cooling	✓
Lower LW_{in} and associated surface cooling	✗
Surface warming due to more heat storage (G) release (JJA)	Surface warming due to more heat storage release (G) (JJA and DJF)

[a]Overview of the biogeophysical mechanisms responsible for observed and modeled δT_s values. Checkmarks indicate that the mechanism present in reality is included correctly in the model (or vice versa). Question marks indicate that we were not able to determine conclusively if the mechanism included in reality was present in the model (or vice versa). Crosses indicate that the mechanism included in reality was missing from the model (or vice versa).

each other perfectly. In the 45°–56°N latitudinal range, albedo-induced cooling is stronger and is able to overcome warming due to turbulent suppression. The daytime-specific δT_a values and the responsible processes reported in this study for European site pairs seem to coincide well with these observed North American values. The mechanisms responsible for the temperature differences are the same mechanisms we discussed when giving an overview of the daily mean effect of deforestation.

Nighttime situations offer a different view. Few studies report nighttime δT_a values, but the ones that do all report that deforestation leads to a nighttime cooling in the order of −1 to −2 K (Table 4). Values for δT_a reported here are similar, at −2 K uncorrected and −1 K with extreme lapse rate correction for the data subset using all site pairs. Both *Lee et al.* [2011] and *Zhang et al.* [2014] also touch briefly on the mechanism responsible for these differences, speculating that open land is cooler at night because forests can bring more heat from aloft to the surface due to increased turbulent mixing. However, neither study provides any evidence backing up this hypothesis. As shown here in section 3.2, the nighttime cooling associated with deforestation observed in our site pairs seems to be the result of a combination of factors. The first mechanism responsible for nighttime cooling is a decrease in incoming longwave radiation. Second, a decrease in turbulent mixing (evidenced by a higher, less negative mean H at night) is observed, confirming the mechanism suggested by *Lee et al.* [2011]. At night, forests thus warm the surface through increased roughness, turbulence and vertical advection. A similar mechanism was reported by *Wouters et al.* [2013] for built-up urban environments.

It is important to note, however, that these studies show that nighttime δT_a values are essential in explaining observed yearly mean δT_a. For example, our results show that without nighttime cooling, yearly mean daily δT following deforestation would be positive instead of slightly below zero. The same is true for the North American site pairs studied by *Lee et al.* [2011] in the 28°–45°N latitudinal range. To conclude, there are clearly important mechanisms at play at night which are unrelated to the mechanisms commonly associated with deforestation in studies which focus only on daily mean effects. These mechanisms are important in explaining daily mean δT_a and should therefore be accounted for.

4.2. Added Value of Methodology Based On Temperature Decomposition

As mentioned in section 1, the methodology as applied in this study, which combines simulations with a coupled land-atmosphere, a direct sensitivity analysis evaluating the changes associated with deforestation, a separate analysis for daytime and nighttime and temperature decomposition is a novel way of evaluating the impact of LUC in climate models. It moves past simple bias description by investigating the biogeophysical mechanisms responsible for surface temperature differences in both model and observations. This is accomplished by calculating the sensitivity of changes in surface temperature to changes in the component of the energy budget, i.e., albedo, latent heat, sensible heat, incoming shortwave radiation, ground heat, and ecosystem emissivity.

The underlying idea of this method is that LUC triggers changes in the biogeophysical interactions between the land surface and the atmosphere. For example, forests have deeper and more complex rooting systems compared to grasses or crops and, therefore, are likely to maintain higher evapotranspiration rates under dry

conditions. This example illustrates that changes in biogeophysical properties following LUC have a direct or indirect impact on one or multiple components of the surface energy budget. In this particular example, the SEB component most affected will be latent heat flux. In turn, any change in a SEB component triggers, if isolated, a change in near surface temperature. For example, higher evapotranspiration rates, if not compensated by changes in other surface energy budget terms, will lead to lower near surface temperatures due to evaporative cooling. Note though that the method decomposes the net effects of LUC. Gross effects and feedbacks resulting in the net effect remain hidden.

The decomposition method described here allows us to determine whether our model gives acceptable results for δT_s following LUC, or in other words whether the model is simulating correct δT_s values for the right biogeophysical reasons. The decomposition method also helps establishing whether incorrect δT_s values are due to large biases in several biogeophysical mechanisms, due to the result of a modest underestimation in just one of the important mechanisms, or alternatively, simply due to one or more observed biogeophysical mechanisms that are not modeled. These results are summarized in Table 5.

For winter days, COSMO-CLM^2 is able to simulate correct δT_s values for the right reasons, with both model and observations showing a similar cooling following deforestation due to higher albedo partially offset by a reduction in turbulent fluxes. For summer days, both model and observations showed warming following deforestation, but the model simulations include a mechanism raising SW_{in} that was not confirmed by the observations.

Nighttime δT_s values were clearly biased, largely underestimating the observed cooling following deforestation. Biases in two distinct mechanisms are responsible for this underestimation: an underestimation of the reduction in LW_{in} and an overestimation of the increase in heat storage release. It is worth noting thought that a third important nighttime mechanism, a decrease in turbulent mixing, was found to be well represented.

4.3. Difference in Nighttime LW_{in}

Why do we observe a lower LW_{in} over open land at night (Figure 7)? One possible explanation is a decrease in water vapor in the nocturnal boundary layer (NBL), compared to forests. It is well known that water vapor acts as a greenhouse gas, limiting the escape of longwave radiation through the atmosphere [*Christy et al.*, 2006]. It can also cause swelling of hygroscopic aerosols, further increasing LW_{in} in situations where there are substantial emissions of aerosols into the NBL [*Nair et al.*, 2011]. However, only limited evidence of lower water vapor content over open land exists in our measurements. Nighttime specific humidity measured over forest and open land (usually only a few meters above vegetation for flux measurement sites) is comparable for the DE1 site pair and is somewhat lower over open land for the IT2 site pair (-0.4 g/kg or -12% in winter and -1.4 g/kg or -14% in summer). No paired humidity measurements exist for the DK1 site pair. The observations thus do not provide conclusive evidence for a decrease in LW_{in} over open land due to decreased water vapor loading. Answering this question more conclusively would require more measurements higher up in the boundary layer.

One other factor which could explain reduced nighttime LW_{in} over open land is a difference in NBL aerosol loading. Most studies into the effect of atmospheric aerosols focus on daytime [e.g., *Bellouin et al.*, 2005; *Takemura et al.*, 2002]. During daytime, aerosols tend to have a cooling effect on surface temperature due to (1) the direct effect of increased scattering and absorption of shortwave solar radiation and (2) the indirect effect on cloud formation (aerosols act as cloud condensation nuclei) [*Yu et al.*, 2002]. There are few studies focusing on the effect of aerosols on nighttime surface climate. One recent study by *Nair et al.* [2011] did focus on nighttime, using a one-dimensional version of a regional climate model to assess the effect of urban aerosols on radiative forcing and surface air temperature. The results showed that urban aerosols have a statistically significant impact on nighttime downwelling longwave radiation at the surface, increasing LW_{in} by 2.7 to 47 W m^{-2}, depending on the scenario used.

We therefore hypothesize that the difference in nighttime LW_{in} observed for site pairs DE1 and IT2 could be related at least in part to a difference in NBL aerosol loading. Forests emit large quantities of biogenic volatile organic compounds (BVOCs) into the atmosphere, which then in turn contribute to the formation of large secondary organic aerosols (SOAs) [*Ehn et al.*, 2014; *Carslaw et al.*, 2010]. Studies for boreal forests (where anthropogenic air pollution is minimal) have shown that these biogenic SOA can have a large local impact

on the radiative budget [*Kurten et al.*, 2003; *Spracklen et al.*, 2008]. Recently, a modeling study has estimated the impact of global historic cropland expansion through BVOC emissions at a cooling equivalent to -0.11 $\pm 0.17\,\mathrm{W\,m^{-2}}$ [*Unger*, 2014]. However, these studies focus mainly on the impact of aerosols on shortwave scattering and cloud formation. So far, a detailed analysis into the impact of biogenic aerosols on nighttime radiative forcing over forests has not yet been performed.

Finally, higher values of nighttime LW_{in} over forests could be related to the enhanced entrainment of warm air reported in the results section. As mentioned above, forests, owing to their higher aerodynamic roughness, generate more turbulence, evidenced by a lower (more negative) mean nighttime sensible heat flux (Figure 6). As shown by *Walters et al.* [2007], any perturbation in a weakly stable nocturnal boundary layer can trigger a shift from a stable temperature profile to a turbulent regime, mixing warm air from aloft and significantly increasing (near) surface temperature. Assuming the advection of warmer air closer to the surface increases surface LW_{in}, the higher nighttime LW_{in} observed over forests could simply be related to the increased occurrence of this type of disruptive events. If true, however, it would mean that COSMO-CLM^2 correctly simulates the mean decrease in H over forests, but not the associated near surface air warming and increase in LW_{in}. One possible reason could be that the vertical resolution used (32 vertical levels for the entire atmosphere) is inadequate, lacking the precision required to simulate these vertical processes in the shallow NBL. Climate model runs at higher vertical resolution are needed to verify this hypothesis.

4.4. Difference in Daytime SW_{in}

The observed reduction in low and midlevel cloud cover may be a response to a reduction in turbulence associated with deforestation. Turbulence can cause convective cloud formation in the boundary layer, especially during summer. However, as shown in Figure 5c, the modeled daytime sensible heat flux over open land is significantly lower than the modeled sensible heat flux over forests, with a mean reduction of about $50\,\mathrm{W\,m^{-2}}$, which could definitely contribute to a reduction in cloud cover. No similar consistent decrease in incoming shortwave radiation during summer days is observed in our FLUXNET site pairs. However, it is worth noting that this could be related to the specifics of the evaluation setup used in this study.

As mentioned previously, we attempt to simulate the difference in forest and open land climate observed in FLUXNET site pairs by modifying the land use of a 25 by 25 km model pixel ($625\,\mathrm{km^2}$). The observational setup, in which we compare flux tower measurements from two separate real world locations, resembles this situation in land use but not necessarily in scale. For example, most forest measurement locations are located in relatively small forest patches (2–$60\,\mathrm{km^2}$) surrounded by open land. The forest patches of site pairs DK1, DE1, and IT2, the three site pairs included in the reliable data subset, are approximately $3\,\mathrm{km^2}$, $60\,\mathrm{km^2}$, and $10\,\mathrm{km^2}$ in size, respectively. The DK1 and DE1 forest patches are surrounded mostly by cropland, the IT2 forest patch is surrounded by a mountainous landscape consisting of forests, grasslands, steep rocky slopes, and villages.

Therefore, we cannot conclude with any certainty that the decrease in convective uplift and associated decrease in cloud cover simulated by COSMO-CLM^2 represents a genuine model bias. Several studies have shown that this mechanism can have a substantial impact when land use is altered on a large scale. For example, in southwestern Australia, a substantial area of approximately $100{,}000\,\mathrm{km^2}$ was cleared for agricultural use (mostly wheat) during the twentieth century, while the natural woodlands to the east were left untouched. Observational studies have shown that the woodlands lower albedo and higher aerodynamic roughness lead to higher convective activity and a deeper boundary layer. Combined with a local circulation pattern bringing in moist air from the wheatlands, this resulted in an increase in convective cloud formation and precipitation (+10%) over the woodlands, and a corresponding decrease in precipitation over the wheatlands (−30%) [*Chambers*, 1998]. Land degradation in the Sahel may have caused a similar shift in local circulation and precipitation, exacerbating the 30 year drought initially triggered by changes in sea surface temperature in the adjacent Atlantic Ocean [*Foley et al.*, 2003; *Lauwaet et al.*, 2009, 2010].

Therefore, regional climate runs at a higher horizontal resolution (e.g., 1–2 km) are necessary to determine whether the difference between modeled and observed SW_{in} is, in fact, caused by a mismatch in LUC scale.

Furthermore, the possible presence of a scale-related bias means the evaluation methodology presented here is not immediately transferable to GCMs, given the strong contrast between the scale of LUC represented by our observational site pairs and the typical resolution currently used for global simulations (100–200 km).

5. Conclusions

In this study, we present a method for evaluating the impact of LUC on surface climate in coupled land-atmosphere climate models. The method uses a paired site approach and differentiates between daytime and nighttime climate. It evaluates both the difference in surface temperature and the underlying mechanisms by applying a radiative surface temperature (T_s) change decomposition equation to both observations and model simulations. We apply it to a state of the art regional climate model used extensively for Europe, namely, COSMO-CLM^2.

Observed differences in 2 m air temperature (δT_a) and radiative surface temperature (δT_s) for European open land and forest site pairs are mostly in line with literature reported values for temperate climate regions and stress the important contribution of nighttime temperature change to the daily mean temperature change signal. However, they are not uniformly reproduced by our climate model. Daytime δT following deforestation is simulated correctly in winter but underestimated in summer. The impact of deforestation on nighttime T_s, namely, a significant cooling, is not captured in the model. Using the δT_s decomposition equation, we were able to identify the underlying reasons by determining which LUC-related biogeophysical mechanisms were well represented in COSMO-CLM^2, and which were not (Table 5).

This analysis showed that nighttime cooling is missing from COSMO-CLM^2 mainly because it does not capture the observed reduction in incident longwave radiation (LW_{in}). We hypothesize three mechanisms that might be responsible for this reduction in LW_{in} over open land in the observations: an aerosol effect related to forest VOC emissions, decreased boundary layer humidity and a reduction in near-surface air warming due to increased nocturnal boundary layer stability. In contrast, two mechanisms responsible for a change in T_s over open land sites are, in fact, adequately represented in COSMO-CLM^2: surface cooling due to a higher (less negative) sensible heat flux and summertime surface warming due to an increase in heat storage release.

For daytime, one biogeophysical deforestation mechanism in particular is responsible for the sign and magnitude of observed δT_s values: surface cooling due to a higher albedo, which is more than compensated by warming due to reduced turbulent fluxes in summer, but only partly compensated by reduced turbulent fluxes in winter. This mechanism proved to be reasonably well represented in COSMO-CLM^2. However, COSMO-CLM^2 includes an additional atmospheric feedback in summer: the reduction in surface aerodynamic roughness and associated decrease in turbulent fluxes reduces convective cloud formation and increases incoming shortwave radiation. There is no evidence for this feedback in the observational data set. This might be due to an issue of scale, as the forested vegetation patches used in the observational data set (2–60 km^2) are considerably smaller than the simulated patches (625 km^2).

Overall, our results highlight the importance of evaluating LUC effects separately for daytime and nighttime conditions rather than for average conditions. Averaged values might not reflect reality if the climate model used contains a nighttime bias similar to what was reported here. To further improve upon the above evaluation, higher-resolution runs (both horizontal and vertical resolution) and more detailed observational data are needed. Especially for nighttime, detailed vertical profiles of temperature, humidity and ideally, aerosol concentrations in the nocturnal boundary layer are needed to determine what mechanisms are responsible for the increase in LW_{in} over forests.

References

Abramowitz, G., R. Leuning, M. Clark, and A. Pitman (2008), Evaluating the performance of land surface models, *J. Clim.*, *21*(21), 5468–5481, doi:10.1175/2008JCLI2378.1.

Akkermans, T., et al. (2012), Validation and comparison of two soil-vegetation-atmosphere transfer models for tropical Africa, *J. Geophys. Res.*, *117*, G02013, doi:10.1029/2011JG001802.

Akkermans, T., A. Van Rompaey, N. Van Lipzig, P. Moonen, and B. Verbist (2013), Quantifying successional land cover after clearing of tropical rainforest along forest frontiers in the Congo Basin, *Phys. Geogr.*, *34*(6), 417–440, doi:10.1080/02723646.2013.855698.

Akkermans, T., W. Thiery, and N. P. M. Van Lipzig (2014), The regional climate impact of a realistic future deforestation scenario in the Congo Basin, *J. Clim.*, *27*(7), 2714–2734, doi:10.1175/JCLI-D-13-00361.1.

Asharaf, S., and B. Ahrens (2013), Soil-moisture memory in the regional climate model COSMO-CLM during the Indian Summer Monsoon season, *J. Geophys. Res., Atmos.*, *118*, 6144–6151, doi:10.1002/jgrd.50429.

Bala, G., K. Caldeira, M. Wickett, T. J. Phillips, D. B. Lobell, C. Delire, and A. Mirin (2007), Combined climate and carbon-cycle effects of large-scale deforestation, *Proc. Natl. Acad. Sci. U.S.A.*, *104*(16), 6550–6555, doi:10.1073/pnas.0608998104.

Baldauf, M., A. Seifert, J. Förstner, D. Majewski, M. Raschendorfer, and T. Reinhardt (2011), Operational convective-scale numerical weather prediction with the COSMO model: Description and sensitivities, *Mon. Weather Rev.*, *139*(12), 3887–3905, doi:10.1175/MWR-D-10-05013.1.

Baldocchi, D., and S. Ma (2013), How will land use affect air temperature in the surface boundary layer? Lessons learned from a comparative study on the energy balance of an oak savanna and annual grassland in California, USA, *Tellus B*, *65*, doi:10.3402/tellusb.v65i0.19994.

Bellouin, N., O. Boucher, J. Haywood, and M. Shekar Reddy (2005), Global estimate of aerosol direct radiative forcing from satellite measurements, *Nature*, *438*(7071), 1138–1141, doi:10.1038/nature04348.

Boisier, J. P., N. de Noblet-Ducoudré, A. J. Pitman, F. T. Cruz, C. Delire, B. J. J. M. van den Hurk, M. K. van der Molen, C. Müller, and A. Voldoire (2012), Attributing the impacts of land-cover changes in temperate regions on surface temperature and heat fluxes to specific causes: Results from the first LUCID set of simulations, *J. Geophys. Res.*, *117*, D12116, doi:10.1029/2011JD017106.

Boisier, J. P., N. de Noblet-Ducoudré, and P. Ciais (2013), Inferring past land use-induced changes in surface albedo from satellite observations: A useful tool to evaluate model simulations, *Biogeosciences*, *10*(3), 1501–1516, doi:10.5194/bg-10-1501-2013.

Boisier, J. P., N. de Noblet-Ducoudré, and P. Ciais (2014), Historical land-use induced evapotranspiration changes estimated from present-day observations and reconstructed land-cover maps, *Hydrol. Earth Syst. Sci. Discuss.*, *11*(2), 2045–2089, doi:10.5194/hessd-11-2045-2014.

Bonan, G. (2008), Forests and climate change: Forcings, feedbacks, and the climate benefits of forests, *Science*, *320*(5882), 1444–1449, doi:10.1126/science.1155121.

Brovkin, V., M. Claussen, E. Driesschaert, T. Fichefet, D. Kicklighter, M. F. Loutre, H. D. Matthews, N. Ramankutty, M. Schaeffer, and A. Sokolov (2006), Biogeophysical effects of historical land cover changes simulated by six Earth system models of intermediate complexity, *Clim. Dyn.*, *26*(6), 587–600, doi:10.1007/s00382-005-0092-6.

Carslaw, K. S., O. Boucher, D. V. Spracklen, G. W. Mann, J. G. L. Rae, S. Woodward, and M. Kulmala (2010), A review of natural aerosol interactions and feedbacks within the Earth system, *Atmos. Chem. Phys.*, *10*(4), 1701–1737, doi:10.5194/acp-10-1701-2010.

Chambers, S. (1998), Short- and long-term effects of clearing native vegetation for agricultural purposes, PhD thesis, Univ. of South Australia, Adelaide, Australia.

Christy, J. R., W. B. Norris, K. Redmond, and K. P. Gallo (2006), Methodology and results of calculating central California surface temperature trends: Evidence of human-induced climate change?, *J. Clim.*, *19*(4), 548–563.

Davin, E. L., and N. de Noblet-Ducoudré (2010), Climatic impact of global-scale deforestation: Radiative versus nonradiative processes, *J. Clim.*, *23*(1), 97–112, doi:10.1175/2009JCLI3102.1.

Davin, E. L., and S. I. Seneviratne (2012), Role of Land Surface Processes and Diffuse/direct Radiation Partitioning in Simulating the European Climate, *Biogeosciences*, *9*(5), 1695–1707, doi:10.5194/bg-9-1695-2012.

Davin, E. L., R. Stöckli, E. B. Jaeger, S. Levis, and S. I. Seneviratne (2011), COSMO-CLM2: A new version of the COSMO-CLM model coupled to the Community Land Model, *Clim. Dyn.*, *37*(9–10), 1889–1907, doi:10.1007/s00382-011-1019-z.

De Noblet-Ducoudré, N., et al. (2012), Determining robust impacts of land-use-induced land cover changes on surface climate over North America and Eurasia: Results from the first set of LUCID experiments, *J. Clim.*, *25*(9), 3261–3281, doi:10.1175/JCLI-D-11-00338.1.

Demuzere, M., K. Oleson, A. M. Coutts, G. Pigeon, and N. P. M. van Lipzig (2013), Simulating the surface energy balance over two contrasting urban environments using the Community Land Model urban, *Int. J. Climatol.*, *33*(15), 3182–3205, doi:10.1002/joc.3656.

Dosio, A., H. J. Panitz, M. Schubert-Frisius, and D. Lüthi (2014), Dynamical downscaling of CMIP5 global circulation models over CORDEX-Africa with COSMO-CLM: Evaluation over the present climate and analysis of the added value, *Clim. Dyn.*, *44*, 2637–2661, doi:10.1007/s00382-014-2262-x.

Ehn, M., et al. (2014), A large source of low-volatility secondary organic aerosol, *Nature*, *506*(7489), 476–479, doi:10.1038/nature13032.

Feldmann, H., G. Schädler, H. J. Panitz, and C. Kottmeier (2013), Near future changes of extreme precipitation over complex terrain in central Europe derived from high resolution RCM ensemble simulations, *Int. J. Climatol.*, *33*(8), 1964–1977, doi:10.1002/joc.3564.

Foken, T. (2008), The energy balance closure problem: An overview, *Ecol. Appl.*, *18*(6), 1351–1367, doi:10.1890/06-0922.1.

Foley, J. A., M. T. Coe, M. Scheffer, and G. Wang (2003), Regime shifts in the Sahara and Sahel: Interactions between ecological and climatic systems in Northern Africa, *Ecosystems*, *6*(6), 524–532, doi:10.1007/s10021-002-0227-0.

Hasler, N., D. Werth, and R. Avissar (2009), Effects of tropical deforestation on global hydroclimate: A multimodel ensemble analysis, *J. Clim.*, *22*(5), 1124–1141, doi:10.1175/2008JCLI2157.1.

Juang, J. Y., G. Katul, M. Siqueira, P. Stoy, and K. Novick (2007), Separating the effects of albedo from eco-physiological changes on surface temperature along a successional chronosequence in the Southeastern United States, *Geophys. Res. Lett.*, *34*, L21408, doi:10.1029/2007GL031296.

Karl, T. R., et al. (1993), A new perspective on recent global warming: Assymetric trends of daily maximum and minimum temperature, *Bull. Am. Meteorol. Soc.*, *74*, 1007–1023.

Keuler, K., K. Radtke, and G. Georgievski (2012), *Summary of Evaluation Results for COSMO-CLM Version 4.8_clm13 (clm17): Comparison of Three Different Configurations Over Europe Driven by ECMWF Reanalysis Data ERA40 for the Period 1979–2000*, Brandenburg Univ. of Technology, Cottbus, Germany.

Kothe, S., D. Lüthi, and B. Ahrens (2014), Analysis of the West African monsoon system in the regional climate model COSMO-CLM, *Int. J. Climatol.*, *34*(2), 481–493, doi:10.1002/joc.3702.

Kotlarski, S., et al. (2014), Regional climate modeling on European scales: A joint standard evaluation of the EURO-CORDEX RCM ensemble, *Geosci. Model Dev.*, *7*(4), 1297–1333, doi:10.5194/gmd-7-1297-2014.

Krinner, G., N. Viovy, N. de Noblet-Ducoudré, J. Ogée, J. Polcher, P. Friedlingstein, P. Ciais, S. Sitch, and I. C. Prentice (2005), A dynamic global vegetation model for studies of the coupled atmosphere-biosphere system, *Global Biogeochem. Cycles*, *19*, GB1015, doi:10.1029/2003GB002199.

Kurten, T., M. Kulmala, M. D. Maso, T. Suni, A. Reissell, H. Vehkamäki, P. Hari, A. Laaksonen, Y. Viisanen, and T. Vesala (2003), Estimation of different forest-related contributions to the radiative balance using observations in Southern Finland, *Boreal Environ. Res.*, *8*(4), 275–285.

Lauwaet, D., K. De Ridder, and N. P. M. van Lipzig (2008), The influence of soil and vegetation parameters on atmospheric variables relevant for convection in the Sahel, *J. Hydrometeorol.*, *9*(3), 461–476, doi:10.1175/2007JHM813.1.

Lauwaet, D., N. P. M. van Lipzig, and K. De Ridder (2009), The effect of vegetation changes on precipitation and mesoscale convective systems in the Sahel, *Clim. Dyn.*, *33*(4), 521–534, doi:10.1007/s00382-009-0539-2.

Lauwaet, D., N. P. M. van Lipzig, N. Kalthoff, and K. De Ridder (2010), Impact of vegetation changes on a mesoscale convective system in West Africa, *Meteorol. Atmos. Phys.*, *107*(3–4), 109–122, doi:10.1007/s00703-010-0079-7.

Lauwaet, D., et al. (2013), Impact of nesting resolution jump on dynamical downscaling ozone concentrations over Belgium, *Atmos. Environ.*, *67*(March), 46–52, doi:10.1016/j.atmosenv.2012.10.034.

Lawrence, P. J., and T. N. Chase (2007), Representing a new MODIS consistent land surface in the Community Land Model (CLM 3.0), *J. Geophys. Res.*, *112*, G01023, doi:10.1029/2006JG000168.

Lee, X., et al. (2011), Observed increase in local cooling effect of deforestation at higher latitudes, *Nature*, *479*(7373), 384–387, doi:10.1038/nature10588.

Lejeune, Q., E. L. Davin, B. P. Guillod, and S. I. Seneviratne (2014), Influence of Amazonian deforestation on the future evolution of regional surface fluxes, circulation, surface temperature and precipitation, *Clim. Dyn.*, *44*, 2769–2786, doi:10.1007/s00382-014-2203-8.

Luyssaert, S., et al. (2014), Land management and land-cover change have impacts of similar magnitude on surface temperature, *Nat. Clim. Change*, doi:10.1038/nclimate2196.

Mahmood, R., et al. (2014), Land cover changes and their biogeophysical effects on climate, *Int. J. Climatol.*, *34*(4), 929–953, doi:10.1002/joc.3736.

Medvigy, D., R. L. Walko, M. J. Otte, and R. Avissar (2013), Simulated changes in Northwest U.S. climate in response to Amazon deforestation, *J. Clim.*, *26*(22), 9115–9136, doi:10.1175/JCLI-D-12-00775.1.

Montes-Helu, M. C., T. Kolb, S. Dore, B. Sullivan, S. C. Hart, G. Koch, and B. A. Hungate (2009), Persistent effects of fire-induced vegetation change on energy partitioning and evapotranspiration in Ponderosa Pine Forests, *Agric. For. Meteorol.*, *149*(3–4), 491–500, doi:10.1016/j.agrformet.2008.09.011.

Nair, U. S., R. McNider, F. Patadia, S. A. Christopher, and K. Fuller (2011), Sensitivity of nocturnal boundary layer temperature to tropospheric aerosol surface radiative forcing under clear-sky conditions, *J. Geophys. Res.*, *116*, D02205, doi:10.1029/2010JD014068.

Nikulin, G., et al. (2012), Precipitation climatology in an ensemble of CORDEX-Africa regional climate simulations, *J. Clim.*, *25*(18), 6057–6078, doi:10.1175/JCLI-D-11-00375.1.

Nogherotto, R., E. Coppola, F. Giorgi, and L. Mariotti (2013), Impact of Congo Basin deforestation on the African monsoon, *Atmos. Sci. Lett.*, *14*(1), 45–51, doi:10.1002/asl2.416.

Oleson, K. W., Y. Dai, G. Bonan, M. Bosilovich, R. Dickinson, P. Dirmeyer, F. Hoffman, P. Houser, S. Levis, and G. Y. Niu (2004), Technical description of the Community Land Model (CLM), *NCAR Tech. Note NCAR/TN-461+STR*, Natl. Cent. for Atmos. Res., Boulder, Colo.

Pitman, A. J., et al. (2009), Uncertainties in climate responses to past land cover change: First results from the LUCID intercomparison study, *Geophys. Res. Lett.*, *36*, L14814, doi:10.1029/2009GL039076.

Pitman, A. J., F. B. Avila, G. Abramowitz, Y. P. Wang, S. J. Phipps, and N. de Noblet-Ducoudré (2011), Importance of background climate in determining impact of land-cover change on regional climate, *Nat. Clim. Change*, *1*(9), 472–475, doi:10.1038/nclimate1294.

Randerson, J. T., et al. (2006), The impact of boreal forest fire on climate warming, *Science*, *314*(5802), 1130–1132, doi:10.1126/science.1132075.

Ruppert, J., C. Thomas, and T. Foken (2006), Scalar similarity for relaxed eddy accumulation methods, *Boundary Layer Meteorol.*, *120*(1), 39–63, doi:10.1007/s10546-005-9043-3.

Snyder, P. K., C. Delire, and J. A. Foley (2004), Evaluating the Influence of Different Vegetation Biomes on the Global Climate, *Clim. Dyn.*, *23*(3–4), doi:10.1007/s00382-004-0430-0.

Spracklen, D. V., B. Bonn, and K. S. Carslaw (2008), Boreal forests, aerosols and the impacts on clouds and climate, *Philos. Trans. R. Soc., A*, *366*(1885), 4613–4626, doi:10.1098/rsta.2008.0201.

Stöckli, R., D. M. Lawrence, G.-Y. Niu, K. W. Oleson, P. E. Thornton, Z.-L. Yang, G. B. Bonan, A. S. Denning, and S. W. Running (2008), Use of FLUXNET in the Community Land Model development, *J. Geophys. Res.*, *113*, G01025, doi:10.1029/2007JG000562.

Takemura, T., T. Nakajima, O. Dubovik, B. N. Holben, and S. Kinne (2002), Single-scattering albedo and radiative forcing of various aerosol species with a global three-dimensional model, *J. Clim.*, *15*(4), 333–352, doi:10.1175/1520-0442(2002)015<0333:SSAARF>2.0.CO;2.

Thiery, W., E. Davin, H. Panitz, M. Demuzere, S. Lhermitte, and N. P. M. Van Lipzig (2015), The impact of the African Great Lakes on the regional climate, *J. Clim.*, doi:10.1175/JCLI-D-14-00565.1.

Unger, N. (2014), Human land-use-driven reduction of forest volatiles cools global climate, *Nat. Clim. Change*, *4*(10), 907–910, doi:10.1038/nclimate2347.

Van den Hurk, B. J. J. M., P. Viterbo, A. C. M. Beljaars, and A. K. Betts (2000), Offline validation of the ERA40 surface scheme, *ECMWF Tech. Memo.*, *295*, 43 pp., Eur. Cent. For Medium-Range Weather Forecasts, Reading, U. K. [Available at http://www.ecmwf.int/publications/library/ecpublications/_pdf/tm/001-300/tm295.pdf.]

Vautard, R., et al. (2013), The simulation of European heat waves from an ensemble of regional climate models within the EURO-CORDEX project, *Clim. Dyn.*, *41*(9–10), 2555–2575, doi:10.1007/s00382-013-1714-z.

Viterbo, P., and A. C. M. Beljaars (1995), An improved land surface parameterization scheme in the ECMWF model and its validation, *J. Clim.*, *8*(11), 2716–2748, doi:10.1175/1520-0442(1995)008<2716:AILSPS>2.0.CO;2.

von Randow, C., et al. (2004), Comparative measurements and seasonal variations in energy and carbon exchange over forest and pasture in South West Amazonia, *Theor. Appl. Climatol.*, *78*(1–3), 5–26, doi:10.1007/s00704-004-0041-z.

Vose, R. S., D. R. Easterling, and B. Gleason (2005), Maximum and minimum temperature trends for the globe: An update through 2004, *Geophys. Res. Lett.*, *32*, L23822, doi:10.1029/2005GL024379.

Walters, J. T., R. T. McNider, X. Shi, W. B. Norris, and J. R. Christy (2007), Positive surface temperature feedback in the stable nocturnal boundary layer, *Geophys. Res. Lett.*, *34*, L12709, doi:10.1029/2007GL029505.

Werth, D., and R. Avissar (2002), The local and global effects of Amazon deforestation, *J. Geophys. Res.*, *107*(D20), 8087, doi:10.1029/2001JD000717.

Werth, D., and R. Avissar (2005), The local and global effects of African deforestation, *Geophys. Res. Lett.*, *32*, L12704, doi:10.1029/2005GL022969.

Wilson, K., A. Goldstein, E. Falge, M. Aubinet, D. Baldocchi, P. Berbigier, C. Bernhofer, R. Ceulemans, H. Dolman, and C. Field (2002), Energy balance closure at FLUXNET sites, *Agric. For. Meteorol.*, *113*(1), 223–243.

Wouters, H., K. De Ridder, M. Demuzere, D. Lauwaet, and N. P. M. van Lipzig (2013), The diurnal evolution of the Urban Heat Island of Paris: A model-based case study during summer 2006, *Atmos. Chem. Phys.*, *13*(17), 8525–8541, doi:10.5194/acp-13-8525-2013.

Yu, H., S. C. Liu, and R. E. Dickinson (2002), Radiative effects of aerosols on the evolution of the atmospheric boundary layer, *J. Geophys. Res.*, *107*(D12), AAC31, doi:10.1029/2001JD000754.

Zhang, M., et al. (2014), response of surface air temperature to small-scale land clearing across latitudes, *Environ. Res. Lett.*, *9*(3), 034002, doi:10.1088/1748-9326/9/3/034002.

Zhou, L., R. E. Dickinson, Y. Tian, R. S. Vose, and Y. Dai (2007), Impact of vegetation removal and soil aridation on diurnal temperature range in a semiarid region: Application to the Sahel, *Proc. Natl. Acad. Sci. U.S.A.*, *104*(46), 17,937–17,942, doi:10.1073/pnas.0700290104.